Effect of annealing and doping with (Mo , V and Ni) elements oxides on structural properties of $BaTiO_3$ thin films

Ass.Professor Dr. Sabah A. Salman
University of Diyala , College of Science , Physics Department

Abstract

In this work, $BaTiO_3$ thin films (pure and doped with oxides MoO_3,V_2O_5 and NiO) were deposited using pulsed laser deposition (PLD) technique with thickness equal to (300nm) on glass and Si (111) substrates at temperature equal to (573K). The effects of annealing at temperatures (673K,773K and 873K) and doping on the structural properties have been investigated. XRD of pure and doped $BaTiO_3$ pellets shows Polycrystalline structure, and exhibited tetragonal structure, with preferential direction (110). The structural properties of the $BaTiO_3$ films prepared on glass substrates before and after annealing have been studied by using XRD technique, these tests show that all the films have amorphous structure at substrate temperature (573K) and after annealing at temperatures (673K,773K and 873K). But in case of Si (111) substrates, the XRD did not detect the crystalline phase before annealing, but annealing at temperature (873K), the XRD detected Polycrystalline structure, and exhibited tetragonal structure of $BaTiO_3$ film . The same occurs with doping films.

The surface morphology of all the deposited films was studied using atomic force microscope (AFM). The grain size of the nanoparticles observed at the surface depended on the annealing temperature, where annealing at temperature (873K) was the best temperature at the films deposits on Si (111) substrates. $BaTiO_3$ films with doping ratio (0.1wt%) of NiO has the smallest grain size equal to (44.69nm). RMS roughness increased with increasing annealing temperature.

Keywords: $BaTiO_3$ thin films, pulsed laser deposition , structural Properties, doping.

Effect of annealing and doping with (Mo , V and Ni) elements oxides on structural properties of $BaTiO_3$ thin films

Ass.Professor Dr. Sabah A. Salman

تأثير التلدين والتشويب بأكاسيد العناصر (Mo , V و Ni) على الخصائص التركيبية لأغشية $BaTiO_3$ الرقيقة

ا.م.د. صباح أنور سلمان

جامعة ديالى- كلية العلوم- قسم الفيزياء

الخلاصة

تم في هذا العمل تحضير أغشية الباريوم تيتانيت الرقيقة النقية والمشوبة بأكاسيد (المولبدينوم,الفناديوم والنيكل) باستخدام تقنية الترسيب بالليزر النبضي بسمك مقداره (300nm) على قواعد من الزجاج والسليكون (111) بدرجة حرارة أساس مقدارها (573K). تم دراسة تأثير التلدين بدرجات حرارة (873K,773K,673K) والتشويب على الخصائص التركيبية. إن حيود الأشعة السينية (XRD) لأقراص الباريوم تيتانيت النقية والمشوبة اظهر بأنها متعددة التبلور وظهور التركيب الرباعي مع هيمنة الاتجاه (110). إن الخصائص التركيبية لأغشية الباريوم تيتانيت المحضرة على قواعد من الزجاج قبل وبعد التلدين قد تمت دراستها باستخدام تقنية حيود الأشعة السينية (XRD), وأظهرت النتائج بأن جميع الأغشية عشوائية التركيب عند درجة حرارة قاعدة (573 K) وبعد التلدين بدرجات حرارة (873K,773K,673K). لكن في حالة القواعد السليكونية (111), فان حيود الأشعة السينية (XRD) لم يظهر أي طور بلوري قبل التلدين, ولكن عند التلدين بدرجة حرارة (873K), فان حيود الأشعة السينية (XRD) اظهر بان غشاء الباريوم تيتانيت متعدد التبلور وذا تركيب رباعي. وكذلك الحال نفسه بالنسبة للأغشية المشوبة.

تم دراسة طبوغرافية السطح لجميع الأغشية المرسبة باستخدام مجهر القوى الذرية (AFM), أن الحجم الحبيبي للجسيمات النانوية التي ظهرت عند السطح اعتمد على درجة حرارة التلدين, وكانت أفضل درجة حرارة تلدين هي (873K) للأغشية المرسبة على القواعد السليكونية (111). امتلكت أغشية الباريوم تيتانيت المشوب باوكسيد النيكل بنسبة تركيز (0.1wt%) اصغر حجم حبيبي حيث بلغت قيمته (44.69 nm). إن خشونة السطح تزداد بزيادة درجة حرارة التلدين.

الكلمات المفتاحية: الأغشية الرقيقة لباريوم تيتانيت , الترسيب بالليزر النبضي , الخصائص التركيبية , التشويب .

Effect of annealing and doping with (Mo , V and Ni) elements oxides on structural properties of $BaTiO_3$ thin films

Ass.Professor Dr. Sabah A. Salman

Introduction

Barium titanate ($BaTiO_3$) was one of the first ferroelectric materials discovered, and also one of the first recognized photorefractive material. It is, to date, the most extensively investigated ferroelectric material [1].

$BaTiO_3$ is a member of the perovskites family, of which the parent member is the mineral $CaTiO_3$, called perovskite. The perovskite family includes other well-known materials such as $KNbO_3$, $KTaO_3$, $PbTiO_3$ and $SrTiO_3$. The general formula of any compound belonging to this family is ABO_3, where A is a monovalent, divalent or trivalent metal and B a pentavalent, tetravalent or trivalent element. From the point of view of practical applications this material is very interesting because it is chemically and mechanically very stable and it exhibits ferroelectric properties at and above room temperature [2]. From the optical applications point of view, $BaTiO_3$ is very interesting because of its high linear and nonlinear electro optic coefficients. It is, a well-known dielectric material which has been used as an insulating material to fabricate MIS structures. It exhibits several advantages and properties such as high charge storage capacity, good insulating property, low leakage current density and high dielectric breakdown strength [3].

Barium titanate ($BaTiO_3$) and other perovskite-type materials are being extensively studied for their potential commercial applications in dynamic random access memories (DRAMs) [4, 5]. Ferroelectric thin films attract wide interest due to its good characteristics of dielectricity, piezoelectricity and pyoelectricity. And surface acoustic wave (SAW) device [6,7].

It has become one of the most important electro ceramics since the discovery of its versatility in multilayer ceramic capacitors (MLCC), positive temperature coefficient of resistance (PTCR), thermistors, piezoelectric sensors, transducers, actuators and ferroelectric random access memories (FRAM) and electro-optic devices[8,9]. Its dielectric maximum is shifted towards room temperature by the compositional substitution and its dielectrics were sensitive to temperature, field strength and frequency, especially near the Curie temperature. $BaTiO_3$ thin films can also be used as dielectrics in an amorphous form, bringing the advantage of a much lower process temperature that is required for crystalline $BaTiO_3$ films

[10,11].In case of thin films $BaTiO_3$ have been prepared by sputtering [12] PLD [13] , sol-gel, MOD [14] and MOCVD [15] .PLD is currently the most important method for preparing epitaxial structures for device physics studies.

Experimental procedure

The $BaTiO_3$ was prepared by using solid state reaction method by mixing BaO and TiO_2 compounds in [1:1] ratio, $BaTiO_3$ doped with ratio (0.1wt%) of (Mo,V and Ni oxide) by using solid state reaction method also. After the end of wet mixing and drying process then the mixtures were pressed to form pellets (1.5cm) diameter by using (5ton) pressure. After that, pellets are sintered at (1223K) for (5hr).

$BaTiO_3$ thin films (pure and doped with oxides MoO_3,V_2O_5 and NiO) were deposited using pulsed laser deposition (PLD) technique.

The pulsed laser deposition experiment was carried out inside a vacuum chamber generally in (10^{-3}Torr) vacuum conditions. The focused Nd:YAG SHG Q-switching laser beam incident on the target surface makes an angle of (45°) with it. The films were deposited on glass substrate at temperature (T_S=573K) with rate of deposition equal to (0.5 nm/sec). The deposition was carried out using a Q switched Nd:YAG laser with a frequency second radiation at (532nm) (pulse width (10 nsec) repetition frequency (6 Hz)), for (250) laser pulse.

Films thickness was measured by using optical interferometer method and found to be (300nm), as deposited $BaTiO_3$ films have been annealed at temperatures (673K,773K and 873K) in air.

In order to study the structural properties, the crystalline structure is analyzed with a SHIMADZU 6000 X-ray diffractometer system which records the intensity as a function of Bragg's angle. The source of radiation is Cu(k_α) with wavelength (λ=1.5406Å), current (30mA) and voltage (40kV). The scanning angle 2θ is varied in the range of (20–60) degree with a speed of (4deg/min).

Where the Bragg condition for diffraction [16]:

$$2d \sin\theta = m\lambda \qquad \ldots\ldots\ldots\ldots\ldots\ldots\ldots\ldots\ldots\ldots\ldots\ldots (1)$$

Where (d) is the interplaner distance, (θ) is the diffraction angle (Bragg's angle), (m) is the order of reflection and (λ) is the wavelength.

The observed variation of the crystallization in the thin films is supported by the study of the grain size. The grain size of the thin films was calculated form defractogram peaks using the Scherrer formula [17]:

$$D = \frac{\lambda}{\beta \cos\theta} \qquad \ldots\ldots\ldots\ldots\ldots\ldots\ldots\ldots\ldots\ldots (2)$$

Where (D) is the grain size, (β) is the full width at half maximum (FWHM).

Lattice parameters (a) and (c) for tetragonal crystal are calculated from X-ray d-spacing's according to equation:

$$\frac{1}{d^2} = \frac{h^2 + k^2}{a^2} + \frac{l^2}{c^2} \qquad \ldots\ldots\ldots\ldots\ldots\ldots\ldots\ldots\ldots\ldots (3)$$

Where h, k, and ℓ refer to the Miller indices of individual reflections.

The morphological surface analysis is carried out employing an atomic force microscope (AFM) (AA3000 Scanning Probe Microscope SPM, tip NSC35/AIBS) from Angstrom Ad-Vance Inc.

Results and discussions

Fig. (1) shows the X-Ray diffraction pattern of $BaTiO_3$ pellet. It can be observed that the pellet has polycrystalline structure in nature and exhibited tetragonal structure. It can be noticed from XRD pattern that the peaks at (2θ=22.541°, 31.949°, 39.291°, 45.708°, 51.31° and 56.585°) referred to (100), (110), (111), (200), (210) and (211) planes direction, respectively. With that the strongest peak occurs for the (110) plane at ($2\theta=31.949^0$). Our results are nearly in agreement with Kumar et *al* [18]. A point of interest is that the preferential orientation is the (110) direction of the powder, this may be due to the layer

stability of the (110) plane which reflects the more relaxed bonds with minimum energy. The XRD shows peaks whose positions were shifted slightly from the data of (JCPDS#050626) [19]. Table (1) shows the experiment and the standard peaks from International Centre for Diffraction Data of $BaTiO_3$.

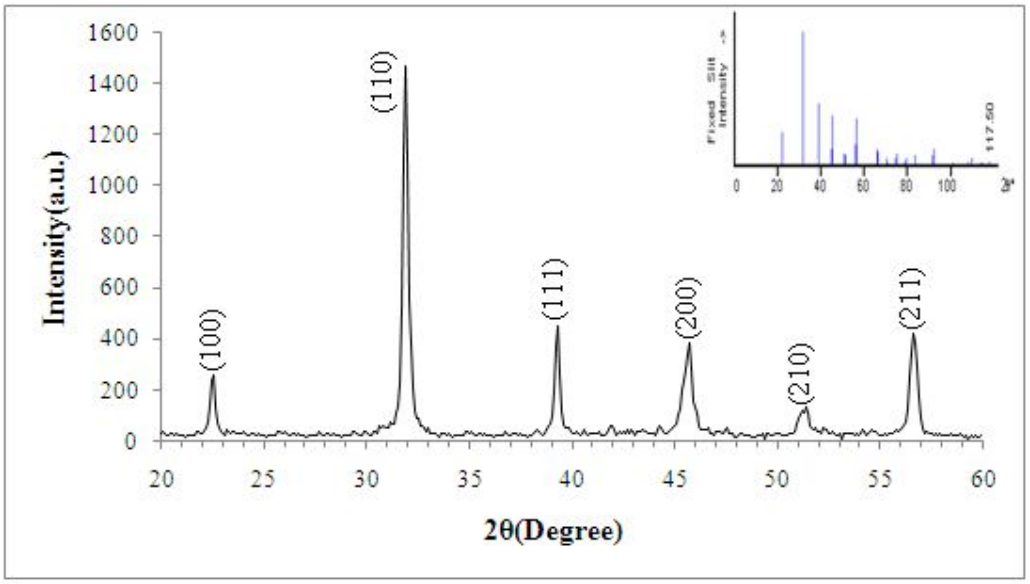

Fig. (1) The XRD pattern of $BaTiO_3$ pellet.

Table (1) The experimental and the standard peaks of $BaTiO_3$ pellet.

2θ Exp.	d Exp.(Å)	d Std.(Å)	Hkl
22.541	3.941	3.99	100
31.949	2.798	2.82	110
39.291	2.291	2.314	111
45.708	1.983	1.99	200
51.31	1.777	1.786	210
56.585	1.625	1.634	211

Figs. (2) to (4) show the X-Ray diffraction pattern of doped $BaTiO_3$ pellets. The composition BaM_xTiO_3 where M=(NiO,MoO_3 and V_2O_5) and x=(0.1wt%). It can be observed that these pellets have polycrystalline structure nature and exhibited tetragonal structure. Fig. (2) shows the XRD pattern of the Ni^{+2} doped BaM_xTiO_3 pellet with the dominant orientation in the (110) direction peak located at (2θ=32.112°). Where as exhibit a prominent reflection angle at (2θ=32.112°) referred to (110) [18]. To form a tetragonal structure according to the International Centre for Diffraction Data (JCPDS#050626) [19]. In Fig. (3) the XRD pattern of the V^{+5} doped BaM_xTiO_3 pellet with the dominant orientation in the (110) direction peak located at (2θ=32.4°). A point of interest is that the preferential orientation is the (110) direction of the powder, this may be due to the layer stability of the (110) a plane which reflects the more relaxed bonds with minimum energy. Another interpretation is that this stability originates in the larger density of bond. Also, Fig. (4) shows the XRD pattern of the Mo^{+6} doped BaM_xTiO_3 pellet with the dominant orientation in the (110) direction peak located at (2θ=32.072°). We can be noticed that there was little shifting of 2θ location to location other. The shift in peak position is due to the variation of atomic radius of the three doping elements as show (Ba=2.22, Ti=1.47, Ni=1.24, Mo=1.39, V=1.34) atomic radius. We can see from Table (2) the experiment values of 2θ shifting for $BaTiO_3$ pellets doped with (NiO,MoO_3 and V_2O_5) and (hkl). Also, Table (3) shows the lattice constants values (a,c and c/a) for $BaTiO_3$ pellets at different doping elements.

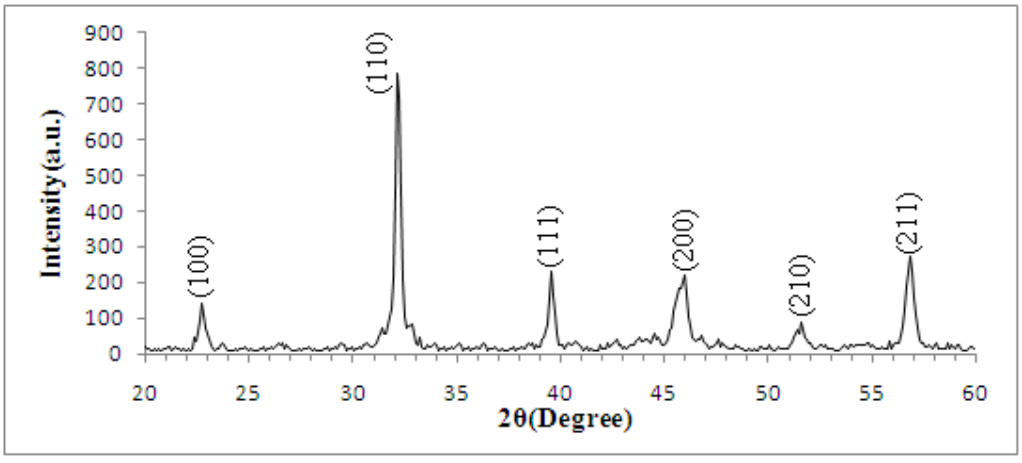

Fig. (2) The XRD pattern of the NiO doped $BaTiO_3$ pellet.

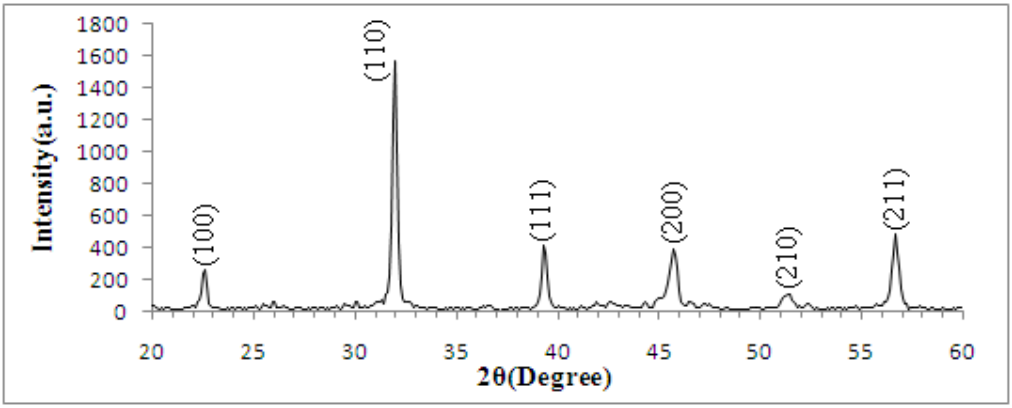

Fig. (3) The XRD pattern of the V_2O_5 doped $BaTiO_3$ pellet.

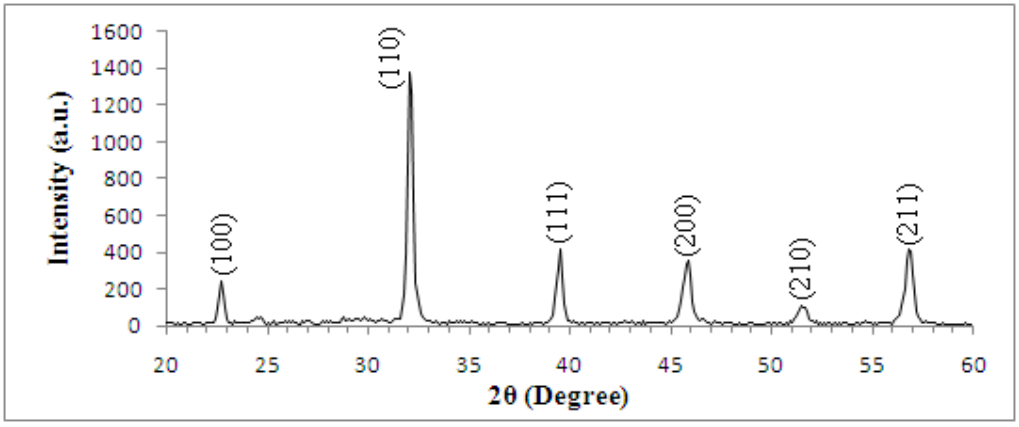

Fig. (4) The XRD pattern of the MoO_3 doped $BaTiO_3$ pellet.

Table (2) The experimental values of 2θ shifting for $BaTiO_3$ pellets doped with (NiO,MoO_3 and V_2O_5) and (hkl).

Doped $BaTiO_3$	2θ(degree)	Hkl	d Exp.(Å)
NiO 0.1wt %	(22.705)	(100)	3.913
	(32.087)	(110)	2.787
	(39.516)	(111)	2.278
	(45.915)	(200)	1.974
	(51.555)	(210)	1.771
	(56.761)	(211)	1.621
MoO_3 0.1wt %	(22.731)	(100)	3.908
	(32.072)	(110)	2.788
	(39.512)	(111)	2.278
	(45.920)	(200)	1.974
	(51.401)	(210)	1.776
	(56.782)	(211)	1.620
V_2O_5 0.1wt %	(22.617)	(100)	3.928
	(32.400)	(110)	2.761
	(39.352)	(111)	2.287
	(45.742)	(200)	1.981
	(51.321)	(210)	1.778
	(56.682)	(211)	1.622

Table (3) The lattice constants values (a,c and c/a) for $BaTiO_3$ pellets at different doping elements.

sample	a (Å)	c (Å)	c/a
$BaTiO_3$	3.957	3.990	1.0080
$BaTiO_3$:0.1wt%NiO	3.941	3.954	1.0032
$BaTiO_3$:0.1wt%MoO_3	3.943	3.956	1.0033
$BaTiO_3$:0.1wt%V_2O_5	3.904	4.083	1.0450

Fig. (5) shows the X-Ray diffraction pattern of $BaTiO_3$ thin films on glass and Si (111) substrates at constant substrate temperature (T_S=573K) and different annealing temperatures (673,773K and 873K). No evidence of any phases present on glass substrate or Si (111) substrate for as deposited thin films, that mean the formation of $BaTiO_3$ phase weak or amorphous that observed from Fig. (5-a,b). Our results are nearly in agreement with Chinchamalatpure et al [3] and Park et *al* [20]. After annealing both samples at temperature (873K), the XRD detected a $BaTiO_3$ on Si (111) substrate but not for glass substrate. All diffraction peaks can be assigned to $BaTiO_3$ phase without any indication of other crystalline phase [3]. We can notice from the XRD pattern that the peaks at (2θ=22.35º, 31.75 º, 39 º, 45.45 º and 56.25 º) referred to (100), (110), (111), (200) and (211) direction, respectively. A point of interest is that the preferential orientation is the (110) direction of the thin film, this may be due to the layer stability of the (110) plane which reflects the more relaxed bonds with minimum energy. The XRD data of thin film coincides with that of the known tetragonal structure according to the International Centre for Diffraction Data (JCPDS#050626) [19]. Also we can notice from the XRD patterns of the $BaTiO_3$ thin films grown on Si (111) substrates diffraction peak located at (2θ=28°) which related to Si wafer. Table (4) shows the experiment and the standard peaks from International Centre for Diffraction Data (JCPDS#050626) [19] of $BaTiO_3$/Si thin film at annealing temperature (873K). The diffraction peaks are broad which indicating the formation of nanocrystalline the average crystal size can calculated as (68nm) from application of Scherer's equation by taking account of the peak broadening at (110) diffraction plane.

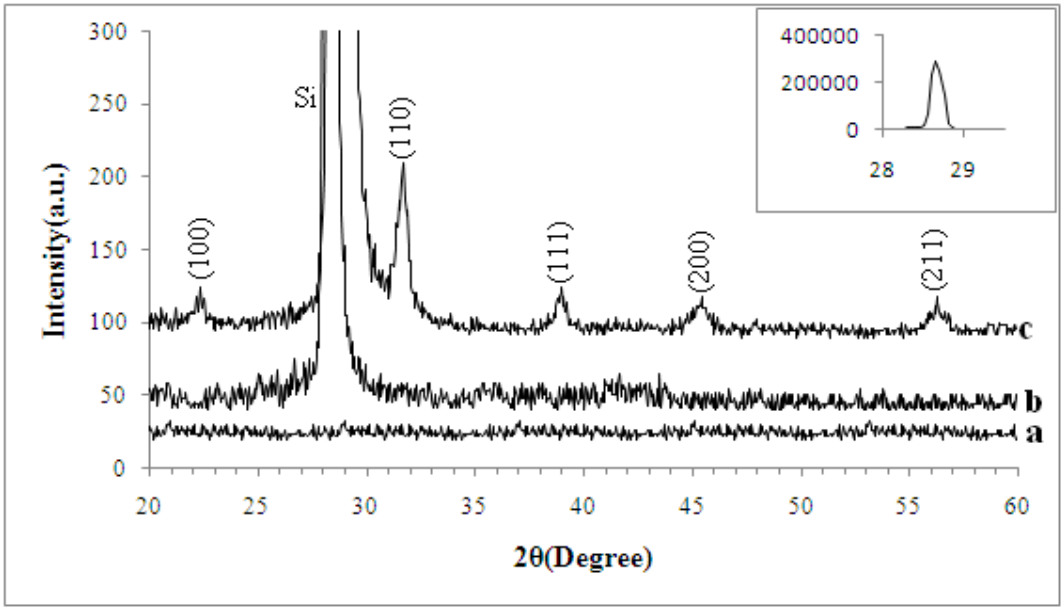

Fig. (5) The XRD pattern of $BaTiO_3$ thin films at:(a) $BaTiO_3$/glass thin film deposited at substrate temperature (T_S=573K), (b) $BaTiO_3$/Si thin film deposited at substrate temperature (T_S=573K), (c) $BaTiO_3$/Si thin film at annealing temperature (873K).

Table (4) The experimental and the standard values of (d,FWHM and Grain size) of $BaTiO_3$/Si thin film at annealing temperature (873K).

2θ Exp.	d Exp.(Å)	d Std.(Å)	hkl	FWHM	main Grain size (nm)
22.35	3.974	3.99	100	0.1183	68.43
31.75	2.816	2.82	110	0.1843	84.66
39	2.307	2.314	111	0.1140	84.94
45.45	1.994	1.997	200	0.1990	43.27
56.25	1.632	1.634	211	0.1822	49.43

Fig. (6) to (8) show the X-Ray diffraction pattern of $BaTiO_3$ thin films doped with different oxides. The composition BaM_xTiO_3 where M=(NiO,MoO_3 and V_2O_5) and x= (0.1wt%) on glass and Si (111) substrates at constant substrate temperature (T_S=573K) and different annealing temperatures (673,773K and 873K). No evidence of any phases present on glass substrates or Si (111) substrates for as deposited thin films, that mean the formation of $BaTiO_3$ phase weak or amorphous. On the other hand, the XRD patterns of doped $BaTiO_3$ thin films with annealing temperature (873K), the structure of these thin films showed a polycrystalline. Fig. (6) shows the XRD pattern of the Ni^{+2} doped BaM_xTiO_3 thin films and exhibited tetragonal structure according to the International Centre for Diffraction Data (JCPDS#050626) [19] . We can be noticed from the XRD pattern that the peaks at (2θ=22.3º, 31.65 º, 39.05 º, 45.35 º, 45.4 º and 56.2 º) referred to (100), (110), (111), (200) and (211) direction, respectively. We can notice that $BaTiO_3$ thin films is present in the (110) at ($2\theta=31.75^0$), such that high peak intensity in (110) direction. Fig. (7) shows the XRD pattern of the V^{+5} doped BaM_xTiO_3 thin films with the dominant orientation in the (110) direction peak located at ($2\theta=31.76^\circ$). Fig (8) shows the XRD pattern of the Mo^{+6} doped BaM_xTiO_3 thin films with the dominant orientation in the (110) direction peak located at ($2\theta=32.7^\circ$). The data indicate a lengthening of the c-axis and shortening of the a-axis to produce a more tetragonal structure. Table (5) shows the experiment values of 2θ shifting for $BaTiO_3$/Si thin films doped with (NiO,MoO_3, and V_2O_5) at annealing temperature (873K) and (hkl). Also, Table (6) shows the lattice constants values (a, c and c/a) for $BaTiO_3$/Si thin films at different doping elements at annealing temperature (873K).

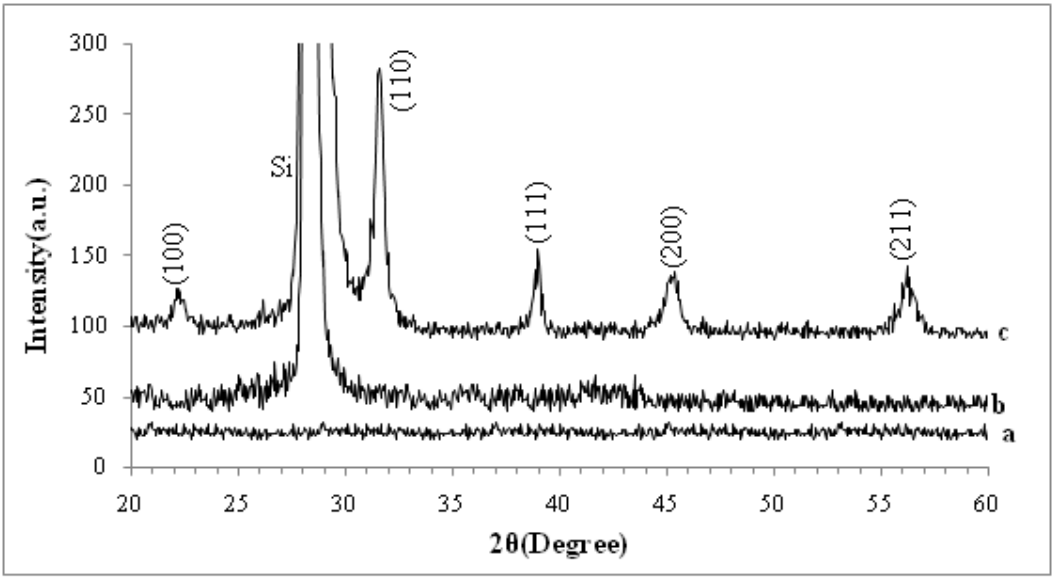

Fig. (6) The XRD pattern at:(a) NiO doped $BaTiO_3$/glass thin film deposited at substrate temperature (T_S=573K), (b) NiO doped $BaTiO_3$/Si thin film deposited at substrate temperature (T_S=573K), (c) NiO doped $BaTiO_3$/Si at annealing temperature (873K).

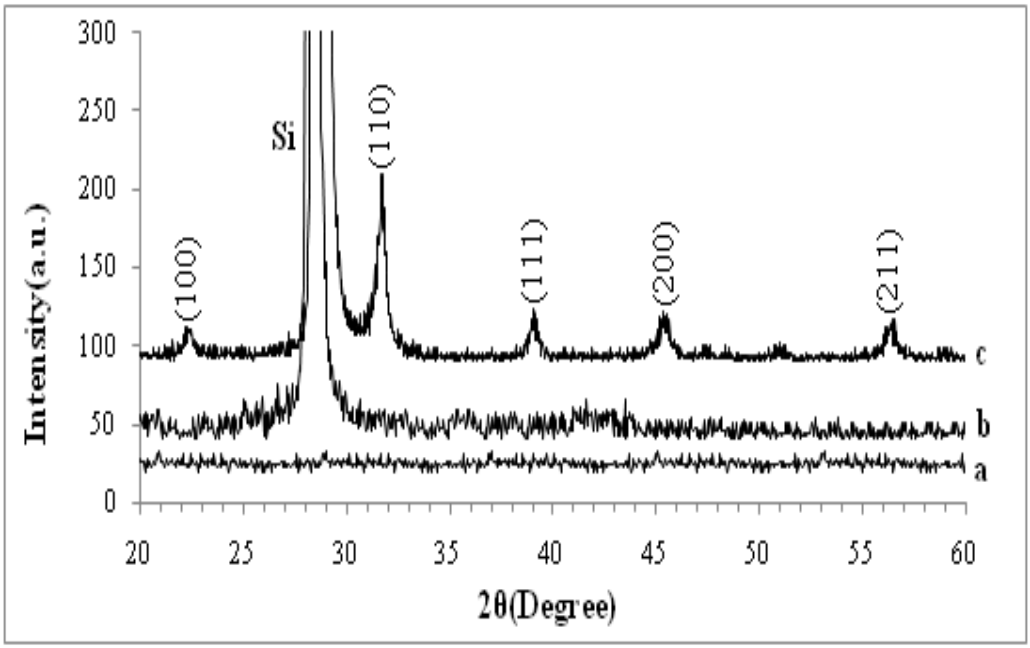

Fig. (7) The XRD pattern at:(a) V_2O_5 doped $BaTiO_3$/glass thin film deposited at substrate temperature (T_S=573K), (b) V_2O_5 doped $BaTiO_3$/Si thin film deposited at substrate temperature (T_S=573K), (c) V_2O_5 doped $BaTiO_3$/Si at annealing temperature (873K).

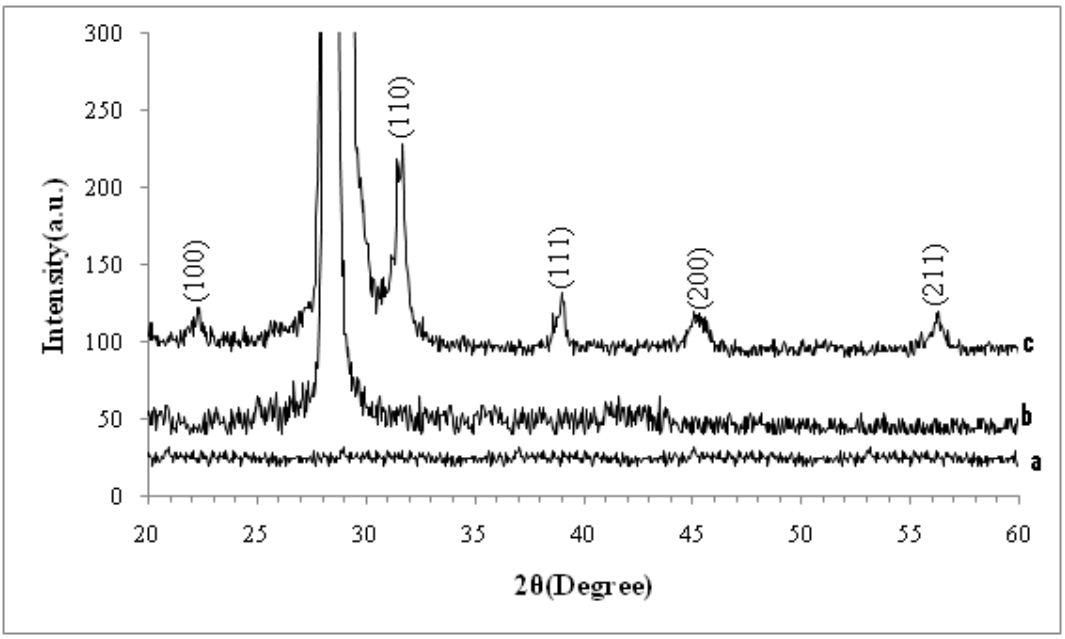

Fig. (8) The XRD pattern at:(a) MoO_3 doped $BaTiO_3$/glass thin film deposited at substrate temperature (T_S=573K), (b) MoO_3 doped $BaTiO_3$/Si thin film deposited at substrate temperature (T_S=573K), (c) MoO_3 doped $BaTiO_3$/Si at annealing temperature (873K).

Table (5) The XRD parameters (2θ,hkl,d exp.,FWHM and Grain size) for $BaTiO_3$/Si thin films doped with (NiO,MoO_3 and V_2O_5) at annealing temperature (873K).

Doped $BaTiO_3$	2θ(degree)	Hkl	d Exp.(Å)	FWHM	main Grain size (nm)
NiO 0.1wt %	(22.3)	(100)	3.983	0.139	58.22
	(31.65)	(110)	2.824	0.143	57.41
	(39.05)	(111)	2.304	0.102	81.97
	(45.4)	(200)	1.996	0.153	56.29
	(56.2)	(211)	1.635	0.170	52.82
	(22.4)	(100)	3.965	0.140	57.68
	(32.7)	(110)	2.736	0.150	54.98

$MoO_3$0.1wt %	(39.05)	(111)	2.304	0.107	78.40
	(45.7)	(200)	1.983	0.273	31.40
	(56.3)	(211)	1.632	0.189	47.60
V_2O_5 0.1wt %	(22.49)	(100)	3.950	0.121	66.68
	(31.76)	(110)	2.815	0.122	67.35
	(39.104)	(111)	2.301	0.117	71.51
	(45.48)	(200)	1.992	0.127	67.7
	(56.6)	(211)	1.624	0.148	60.64

Table (6) The lattice constants values (a,c and c/a) for $BaTiO_3$/Si thin films at different doping elements at annealing temperature (873K).

sample	a (Å)	c (Å)	c/a
$BaTiO_3$	3.982	4.0230	1.010
$BaTiO_3$:0.1wt%NiO	3.995	4.0013	1.015
$BaTiO_3$:0.1wt%MoO_3	3.988	4.0000	1.003
$BaTiO_3$:0.1wt%V_2O_5	3.981	3.9940	1.003

The surface morphology of the undoped $BaTiO_3$ thin films as observed from the AFM micrograph confirms that the grains are uniformly distributed within the scanning area (429nm x 429nm). An initial visual investigation of the deposited thin film on both substrates have shown that they are compact and have good adherence to the substrate. No evidence of cracking observed when the thin film was annealed at temperature (873K). Fig. (9) shows nanostructure $BaTiO_3$ thin films have been deposited on glass and Si (111) substrates at substrate temperature (573K) and annealing temperatures (773K,873K). We can notice that $BaTiO_3$/glass thin film deposited at substrate temperature (573K) is amorphous, while the nanostructure for thin films at the annealing temperatures (773K,873K). It is observed where the RMS roughness value for thin film deposited at substrate temperature (573K) is (0.1nm), while the RMS roughness for thin films annealed at temperatures (773K,873K) is (0.25

nm,0.571nm), respectively as in Fig. (10). Our results are nearly in agreement with Torres-heredia et al [21]. This result indicates that the growth of larger grains with increasing annealing temperature leads to an increase in the surface roughness. The grain size of the thin film can also be deduced from the AFM. It is observed that the average grain size increases with increasing of annealing temperature and the values of the average grain size variable from (48.8nm-58.13nm) when depend at difference annealing temperature. Our results are nearly in agreement with Reddy et al [22].

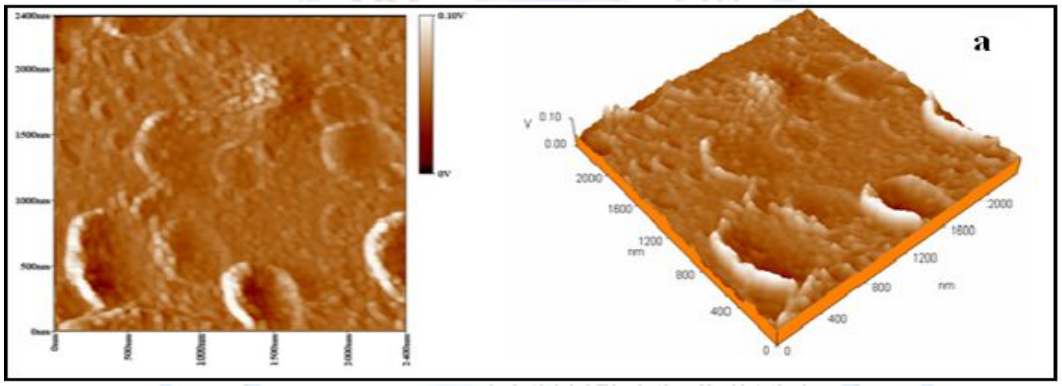

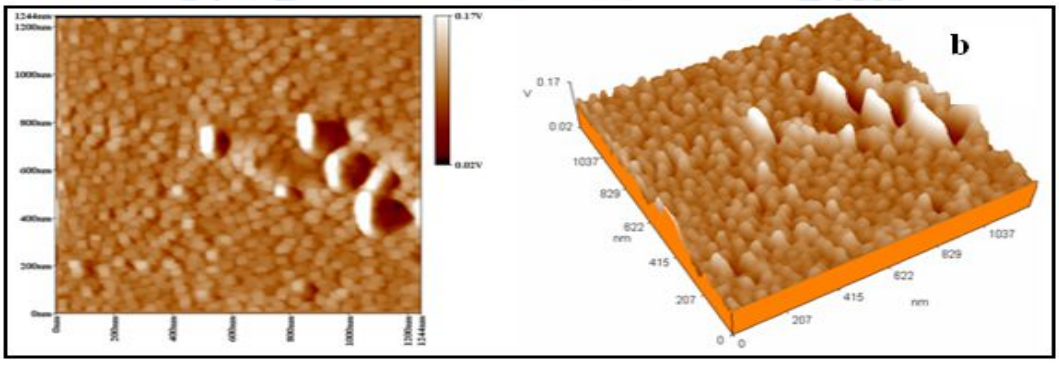

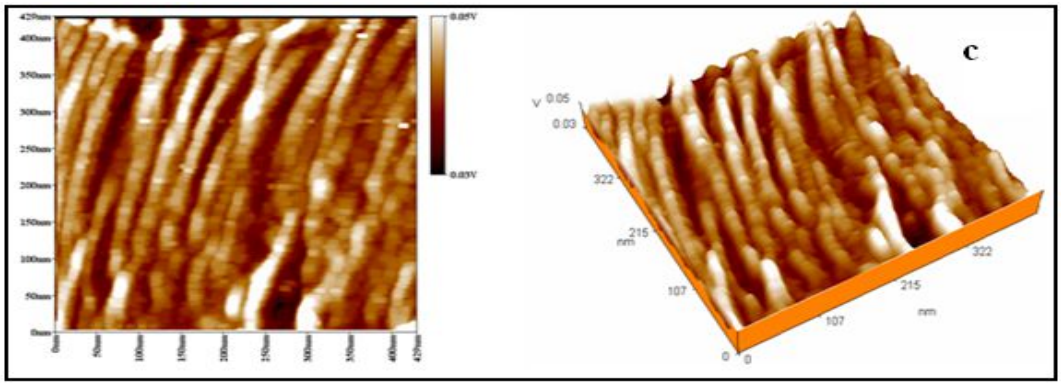

Fig. (9) The AFM images: (a) $BaTiO_3$/glass thin film deposited at substrate temperature (T_S=573K), (b) $BaTiO_3$/glass thin film at annealing temperature (773K), (c) $BaTiO_3$/Si thin film at annealing temperature (873K).

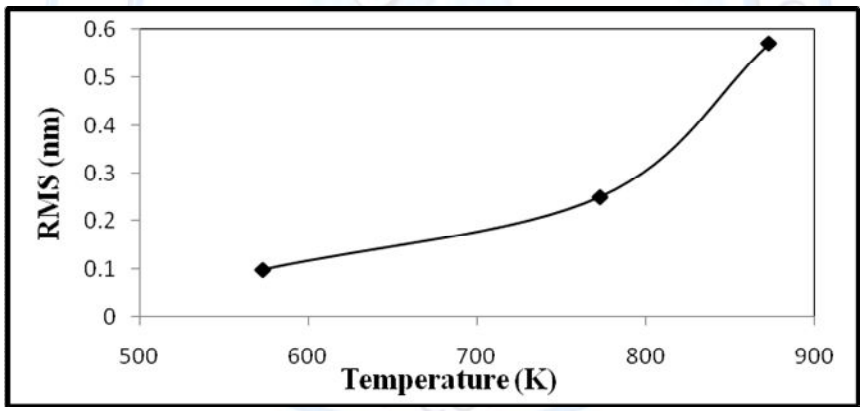

Fig. (10) RMS variation as a function of temperature for different annealing temperatures of $BaTiO_3$ thin films.

Fig. (11) shows the $BaTiO_3$/glass thin films deposited at constant substrate temperature (T_S=573K) with different elements of mixed oxides (NiO,MoO_3 and V_2O_5) with doping ratio (0.1wt%). It has been found that (MoO_3) doped $BaTiO_3$/glass thin film was more uniform than (NiO and V_2O_5). Also, It is observed that the RMS roughness values for different dopants (MoO_3,V_2O_5 and NiO) are (0.5nm,2.77nm and 0.273nm), respectively. Fig. (12)

shows nanostructure doped $BaTiO_3$/Si thin films at annealing temperature (873K) for different elements of mixed oxides (NiO,MoO_3 and V_2O_5) with doping ratio (0.1wt%). It is observed that the RMS roughness increased with different dopants (MoO_3,V_2O_5 and NiO) to have values of (0.569nm,5.27nm and 2.13nm) respectively.

Table (7) The grain size and roughness for undoped and doped $BaTiO_3$/Si thin films at annealing temperature (873K) obtained from AFM and XRD analysis.

Sample	AFM of plane grain size (nm)	RMS roughness(nm)	X-ray of plane grain size (nm)
$BaTiO_3$	58.13	0.571	68.43
$BaTiO_3$:0.1wt%NiO	44.69	2.130	58.22
$BaTiO_3$:0.1wt%MoO_3	54.34	0.569	57.68
$BaTiO_3$:0.1wt%V_2O_5	52.79	5.270	66.68

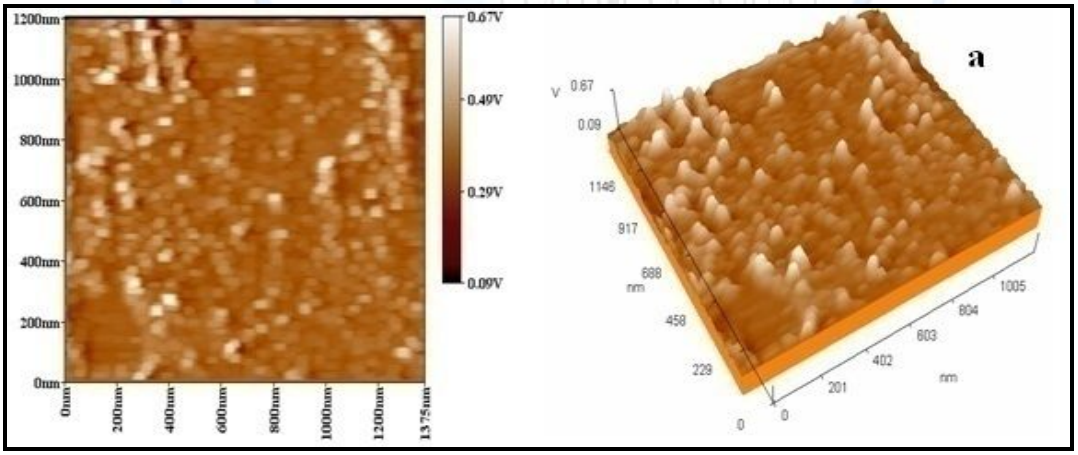

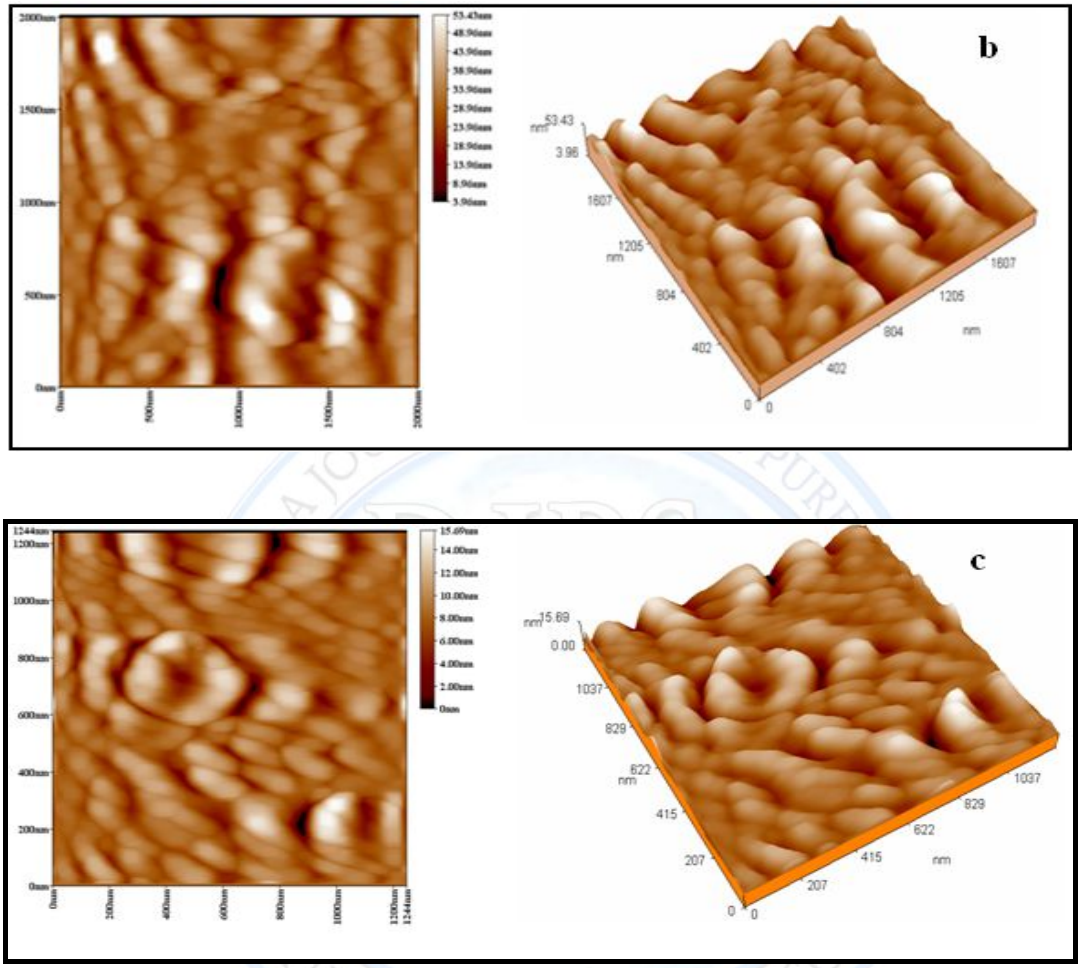

Fig. (11) The AFM images of $BaTiO_3$/glass thin films deposited at substrate temperature (T_S=573K): (a) MoO_3 doped $BaTiO_3$/glass thin film (b) V_2O_5 doped $BaTiO_3$/glass thin film (c) NiO doped $BaTiO_3$/glass thin film.

Effect of annealing and doping with (Mo , V and Ni) elements oxides on structural properties of $BaTiO_3$ thin films

Ass.Professor Dr. Sabah A. Salman

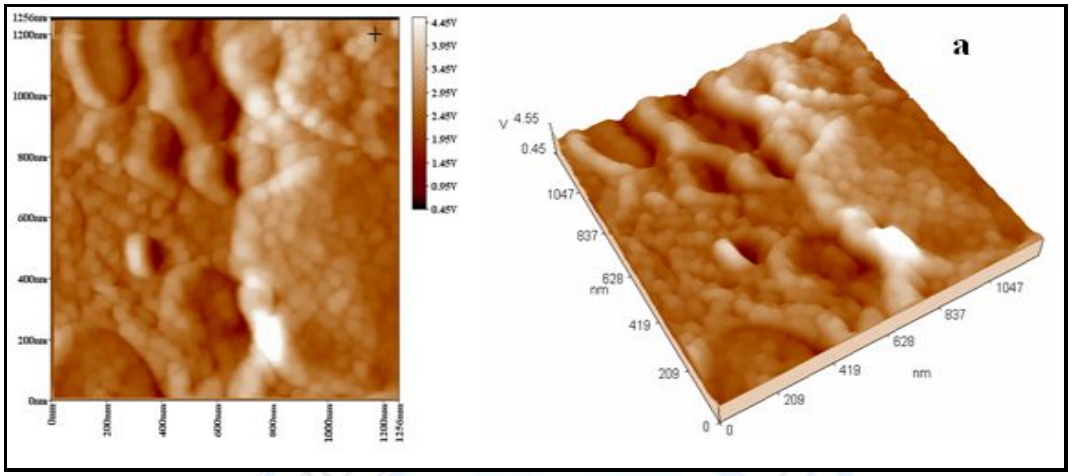

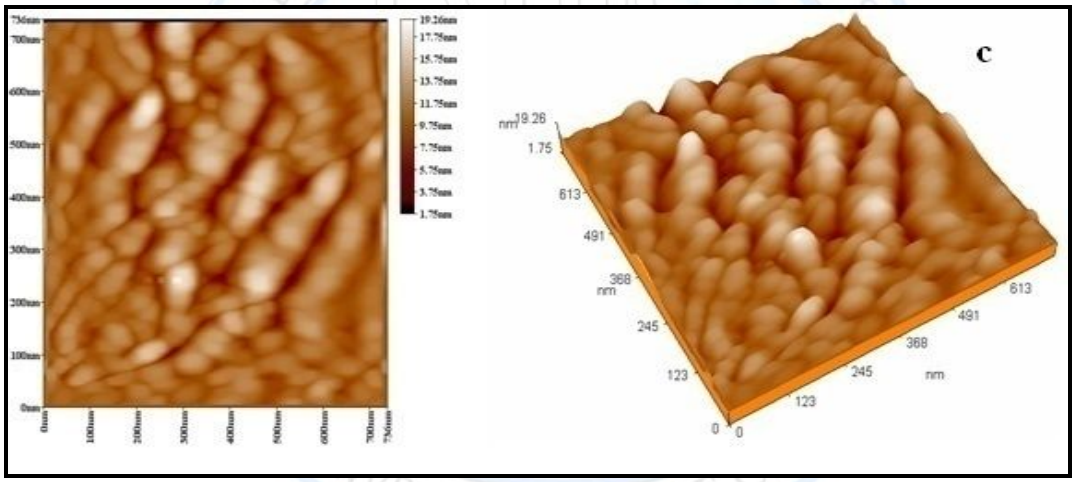

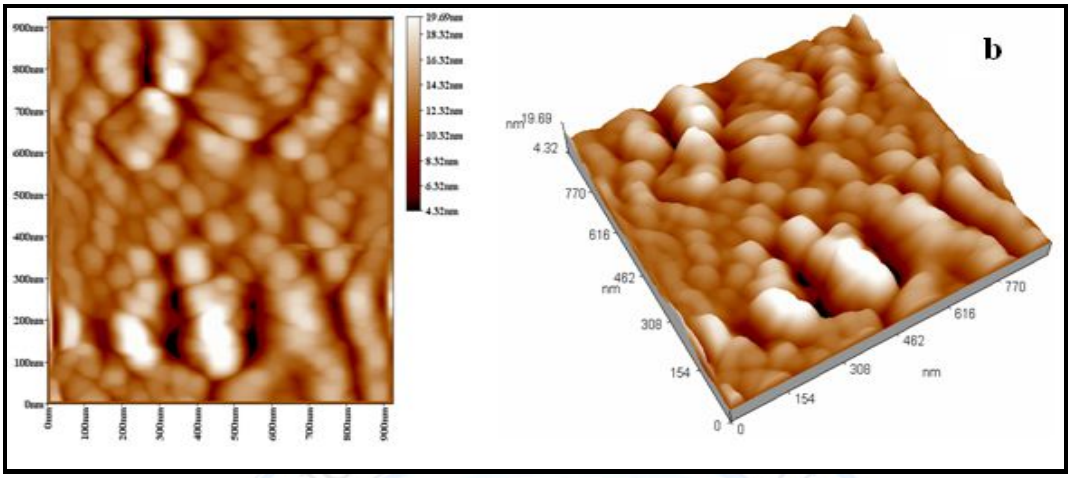

Fig. (12) The AFM images of $BaTiO_3$/Si thin films at annealing temperature (873K): (a) MoO_3 doped $BaTiO_3$/Si thin film (b) V_2O_5 doped $BaTiO_3$/Si thin film (c) NiO doped $BaTiO_3$/Si thin film.

Conclusions

The crystal structure of the $BaTiO_3$ thin films is amorphous for glass and Si (111) substrates then changes to Polycrystalline after annealing process at temperature (873K) for Si (111) substrate only. The same occurs with doping thin films.

The results from AFM of $BaTiO_3$/glass and /Si thin films indicates that the growth of larger grains with increasing annealing temperature leads to an increase in the surface roughness. It is observed that the average grain size increases with increasing of annealing temperature, also the RMS roughness increased with increasing annealing temperature.

The results from AFM of $BaTiO_3$/Si thin films at annealing temperature (873K) for different elements of mixed oxides with doping ratio (0.1wt%), NiO has the smallest grain size.

References

1. M.B.Klein, "Electro-optic and Photorefractive Materials", P.Günter, ed, Springer-Verlag, Berlin, (1986).
2. Y.Xu, "Ferroelectric Materials and Their Application", Elsevier Science Pub.Co., Amsterdam-New York, (1991).
3. V.R.Chinchamalatpure, S.A.Ghosh and G.N.Chaudhari, "Materials Sciences and Applications", Vol.1, p.187, (2010).
4. H.B.Sharma, H.N.K.Sarma and A.Mansingh, J.Appl.Phys., Vol.85, p.341, (1999).
5. B.H.Hoerman, G.M.Ford, L.D.Kaufmann and B.W.Wessels, Appl.Phys.Lett., Vol.73, No.16, p.2248, (1998).
6. R.G.Hunsperger, "Integrated Optics: Theory and Technology", (1992).
7. B.E.A.Saleh and M.C.Teich, "Fundamentals of Photonics", (1991).
8. K.Uchino, "Ferroelectric Devices", Marcel Dekker, Inc., New York, (2000).
9. G.H.Haertling, J.Am.Ceram.Soc., Vol.82, p.797, (1999).
10. K.Sreenivas, A.Mansingh and M.Sayer, J.Appl.Phys. Vol.62, p.4475, (1987).
11. P.Gonon and F.El Kamel, J.Appl.Phys., Vol.101, p.073901, (2007).
12. J.W.Jang, S.J.Chung, W.J.Cho, T.S.Hahn and S.S.Choi, J.Appl.Phys., Vol.81, p.6323, (1997).
13. L.Beckers, J.Schubert, W.Zander, J.Ziesmann, A.Eckau, P.Leinenbach and C.Buchal, J. Appl.Phys., Vol.83, p.3305, (1997).
14. R.W.Schwartz, Chem.Mater., Vol.9, p.2325, (1997).
15. B.S.Kwak, K.Zhang, E.P.Boyd, A.Erbil and B.J.Wilkens, J.Appl.Phys., Vol.69, p.767, (1991).
16. "Fundamentals of the Physics of Solids", Vol.I Structure and Dynamics Translated by Attila Piroth, p.242.
17. O.P.Agnilotriand and B.K.Gupta, J.Appl.physics, Vol.18, p.317, (1979).
18. Y.Kumar, M.A.Mohiddon, A.Srivastava and K.L.Yadav, Indian Journal of Engineering and Materials sciences, Vol.16, p.390, (2009).
19. JCPDS-International Centre for Diffraction Data. PCPDFWIN, Vol.1, No.30, (1997).

20. S.S.Park, J.H.Ha, and H.N.Wadley, "Integrated Ferroelectrics", Vol.95, p.251, (2007).
21. V.Torres-Heredia, J.Munoz-Saldana, F.J.E.Beltran, A.M.Herrera and A.Z. Navarro, Journal of Materials online November, Vol.1, p.1, (2005).
22. Y.K.V.Reddy, D.Mergel, S.Reuter, V.Buck and M.Sulkowski, Journal of physics D: Appl.Phys., Vol.39, p.1161, (2006).